Sensors & Transducers, Vol. 228, Issue 12, December 2018, pp. 30-47

www.sensorsportal.com

Sensors & Transducers

Published by IFSA Publishing, S. L., 2018
http://www.sensorsportal.com

Utilization of the Flexible Fractional Josephson Toroidal Arrays for Sensing, Memory Storage and Quantum Computing

[1] E. T. CHEN, [2] J. T. THORNTON, [3] P. T. KISSINGER, [4] S.-H. DUH

[1] Advanced Biomimetic Sensors, Inc., 11140 Rockville Pike, Suite 440, Unit 422, Rockville, MD 20852, USA
[2] Bruker Nano, 19 Fortune Dr., Billerica, MA 01821, USA
[3] Department of Chemistry, Purdue University, West Lafayette, IN 47906, USA
[4] University of Maryland Medical System, 22 South Greene St, Baltimore, MD 21201, USA
Tel.: 240-706-5687, fax: 240-630-4051
[1] E-mail: ellenchen@nanobiomimeticsensors.com

Received: 11 June 2018 /Accepted: 1 October 2018 /Published: 31 December 2018

Abstract: Self-powered Flexible Fractional Toroidal Josephson Junction (FFTJJ) qubits devices for sensing, memory storage and quantum computing were developed under the conditions of the external magnetic field-free, and operated at room temperature. It mimicked the innate Matrix Metalloproteinase-2 (MMP-2) based on a self-assembling organometallic superlattice membrane on gold chips. The functions of the FFTJJ membrane initiated the intrinsic magnetic flux accompanied with phase change that promoted the superconducting quantum computing function with sensing and quantum computing in the presence of collagen as an analyte and an insulator. The slope value of Josephson Frequency vs. Josephson Shapiro step voltages over different scan rates is a half of the Josephson Constant K_J, indicating the fractional Josephson Effect occurred based on the Direct Electron-Relay (DER) vortices arrays observed at the first time. The FFTJJ dynamic multiple-variable study between differentiate conductivity, inductive energy and charge energy was conducted for use with or without collagen. The experimental results presented in dynamic maps enabled us to confirm that per unit of the inductive energy contributed more to the superconductivity than per unit of the charge energy contribution.

.

Keywords: Flexible Fractional Toroidal Josephson Junction (FFTJJ) Qubits, Nanostructured Biomimetic Matrix Metalloproteinase-2 (MMP-2) Membrane Superlattice, Direct Electron-Relay (DER) Vortices Arrays, Superconductive Quantum Computing and Sensing, Multiple-variable Factor Study, Self-powering.

1. Introduction

The quest for room temperature superconductivity has gripped researchers all over the world for decades since they saw the possibility that the electronic devices can operate more efficiently without energy dissipation [1-4]. The room temperature superconductor has been viewed as a "Holy Grail" that may revolutionize the electronic industries [1-4]. Superconductor qubits are vulnerable to low frequency noise with sources that come from 1/f noise, wave dephasing noise, flux noise, critical current noise, quasiparticle tunneling noise and capacitance noise [5-6]. The nature of the qubits operating multiple states at the same time is more sensitive to decoherence caused by the control and

readout circuitry and the environmental noise as well as to the qubits intrinsic in low frequency noise of conventional computing [5-6]. Building error-tolerant qubits is one of the leading directions to achieve quantum computing [7]. It is well recognized that controlling the fractional quantization has been greatly anticipated for enhancing quantum computing and for advancing quantum science and technology [8-13]. In general, the fractional Josephson Effect possesses a well known 4π periodicity vortex rather than a 2π in the long Josephson junction (LJJ) vortex with or without Majorana zero mode (MZM) [7]. In recent decades, more fractional Josephson Effect systems were theoretically or experimentally reported, which are comprised of one or two vortices [8-9, 14]. Driving by the applications of fractional Josephson junction, such as a two-vortex model system, was proposed for a macroscopic qubit for quantum computing [9]. Amongst the discoveries, p-wave and d-wave molecules were chosen to build the fractional Josephson π-junction [9, 12-13, 15]. Nevertheless, significant progress has been made. However, very few, if any pay attention to the realistic routine practice of using the fractional Josephson Junction technology for sensing self-powering and no energy dissipation quantum computing at one device system in order to eliminate the conventional approaches that transfer data between memory chip and qubit chip. Further, using the microwave power supply caused extreme heat dissipation. The goal of this research project is to develop a new type of qubit system having multiple functions in sensing, memory, energy storage for self- powering and for quantum computing on one single chip based on a flexible d-wave fractional Josephson toroidal array junction approach.

This report is inspired by our prior published literature on developing a nanostructure biomimetic Matrix Metalloproteinase-2 (MMP-2) superconductive, memristive memcapacitive and meminductive device for sensing fg/mL collagen under antibody-free and reagent free conditions by utilizing an approach that used collagen as an analyte and also used it as an unique Josephson toroidal junction barrier to promote Direct Electron-Relay (DER) in a superlattice organo-metal membrane [16-17] at an innate state without denaturing the protein. Its purpose is to further explore the utility of the fractional Josephson vortices arrays, if any, to promote multiple types of sensing, energy storage, and quantum computing at room temperature, also under antibody-free and reagent-free conditions.

2. Results and Discussions

2.1. The Flexible Fractional Josephson Vortices (FFJV)

The Fractional Josephson Vortices (FJV) are used for the purposes of (1) as a magnetic flux quantum system having a non 2π x integer phase winding, i.e., fractional phase winding in heterogeneous interfaces between two superconductors with a barrier through a weak Josephson junction; (2) as an uniform multi-component superconductors which allow integer phase winding 2πN, where N= ±1, ±2..., which carry arbitrarily fractional quantized magnetic flux [18-19]. Our proposed Flexible FJV is defined as a superconductive system which has either superconductive-insulator-superconductive (SIS), or superconductive-normal metal-superconductive (SNS), or superconductor-insulator-memelement (SIM) configuration with barriers such as dielectric insulator, air, transitional metal and conductive polymer with at least one or more inserting spatial locations in the device as shown in Fig. 1. This report attempts to utilize the concept of the Flexible Fractional Toroidal Josephson Junction (FFTJJ) through out the contents to illustrate its applications and uniqueness.

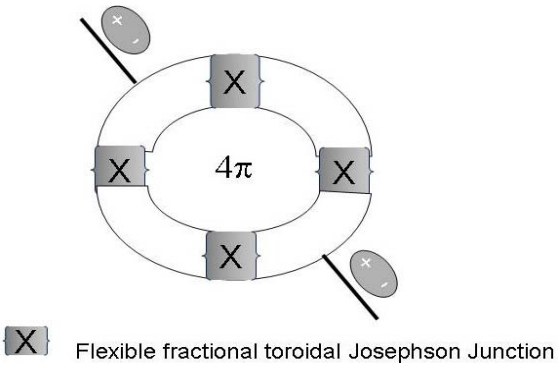

Fig. 1. Depicts the FFTJJ symbol with reversible connection leads.

2.2. An Engineering Design of the Qubit Module

Fig. 2 depicts an art model of a Qubit module comprised of a FFTJJ component.

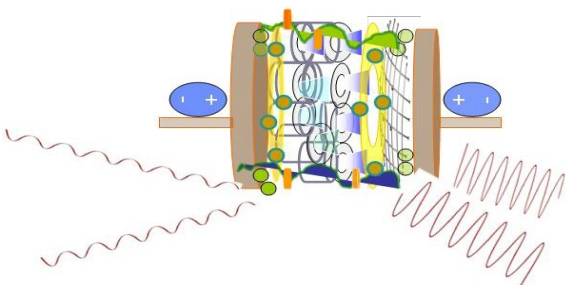

Fig. 2 Depicts the art module of the FFTJJ device. Green circles are the cooper-pairs; the brown balls are symbolic circular current; the horizontal green leaf is the C-terminal; the navy blue leaf is the N-terminal of the polymers; the toroidal arrays are the cyclodextrin cavities; the mash is the dielectric collagen-1.

One Membrane Electrode Assembly (MEA) has a self-assembling organo-metal polymer comprised of triacetyl-ß-cyclodextrin (TCD), polyethylene glycol diglycidyl ether (PEG), poly(4-vinylpyridine) (PVP), bis-substituted dimethyl-β-cyclodextrin (bM-β-DMCD), cysteine and embedded zinc chloride on gold chip. The membrane mimics the innate MMP-2, and the nanostructure superlattice image was shown in Fig. 3A and Fig. 3B. Zinc atom clusters were seen in the AFM images. Zinc atoms serve as the superconducting barrier; and another dielectric collagen barrier- a collagen solution was injected into the assembly module), herein the components of the Membrane Electrode Assembly (MEA) were reversibly connected including the Josephson junction barriers. Friedel-oscillation is a phenomenon for long-range indirect interactions between electrons on the surface based on AFM images [20]. It is well known that superlattice membranes having the Friedel-oscillation can be used as candidates for applications in superconductivity [20]. The observation of the Friedel-oscillation in the membrane was a confirmation of the Cooper-pairs hopping-flip existence. Details were referenced in the literature [16-17].

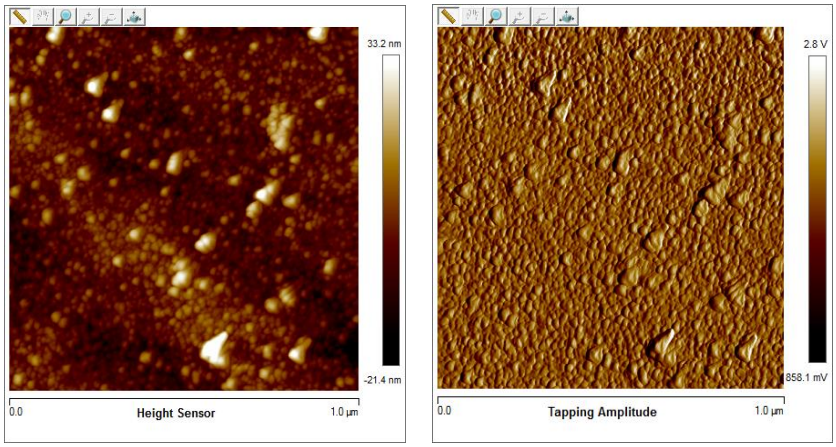

(A) (B)

Fig. 3. (A) Depicts the AFM image of Device 1 at the innate state. (B) Depicts the AFM image at tapping mode.

3. The Sensing Power by the FFTJJ Device

3.1. Calibration of FFTJJ Magnetic Flux

Inspired by the theoretical prediction of a π-phase difference on a topological-superconductor, (TSC)/normal metal (NM) can arise induced by Majorana spin-triplet pairing, which exhibits a Josephson phase of 0 and π-junction in its ground state without any applied magnetic flux [10]. Use of superconducting quantum interference devices (SQUIDs) to sense the magnetic flux, for example, to sense magnetocardiogram signals was reported everywhere; however, under the cryogenic condition requirement, it is not so popular for widespread clinical use [21]. A DC SQUID utilized d-wave $d_{x^2-y^2}$ symmetry and two-π junction interfometer was experimentally realized [22]. The self-induced oscillation between the zero-filed super current by d-wave and the Josephson frequency at the FJV observed in the i-V curve reported in the above cited literature was 4.2-77 K. Our experiment results show the d-wave cross points in hysteretic occurred with the scan rate 1 Hz, 60 Hz and 300 Hz, respectively, and that the Shapiro steps in PBS solution under zero external applied magnetic field at room temperature were observed in Fig. 4A.

The Shapiro Step is a phenomenon that the Cooper pair tunnels in the JJ tunnel with steps that look like a saw tooth. It rises from the response of the super current that oscillating occurred at voltage equal to $nhf/(2e)$, n is an integer, h is Plank's constant, e is the electron when a photon of frequency f or a high frequency current is applied on the JJ tunnel. A dc i-V curve or an ac Josephson current oscillating with the applied frequency gave rise to constant voltage in the i-V curve. The Shapiro step occurs at voltages = nf/K_J, where K_J is the Josephson constant, f is the Josephson frequency. K_J =483.5979 THz/V, is an internationally defined constant, equal to 2e/h, which is the inverse of the single magnetic flux quanta, i.e., $1/\Phi_0$. This effect is used as the Josephson voltage standard [23-24]. Under a FFTJJ situation, Fig. 4B depicts the calibration curve of the Josephson frequency in the range between 6.5 MHz to 0.77 THz vs. Shapiro step voltage between 23 nV to 3 mV over scan rate 1 to 300 Hz. The slope value given the K_J value is that of 483.5979 divided by 2, indicating our system is a 4π FFTJJ vortex [18, 25].

The Shapiro step voltage not only is a function of the Josephson frequency with the linear relationship but also, accompanied with the phase change, was depicted in Fig. 4C at 300 Hz with three cross-points of the FFTJJ at 1.45π, 2.22π and 2.55π, respectively. Noticed, none of the cross-points of the phase discontinuity happened at 0 and π spatial position as the conventional fractional 4π Josephson Effect happens because the intrinsic bidirectional polarity of the electron-relay (evidence given in next Section) around the discontinuity point was asymmetric; hence, the overall vortices array displayed irregular phase change.

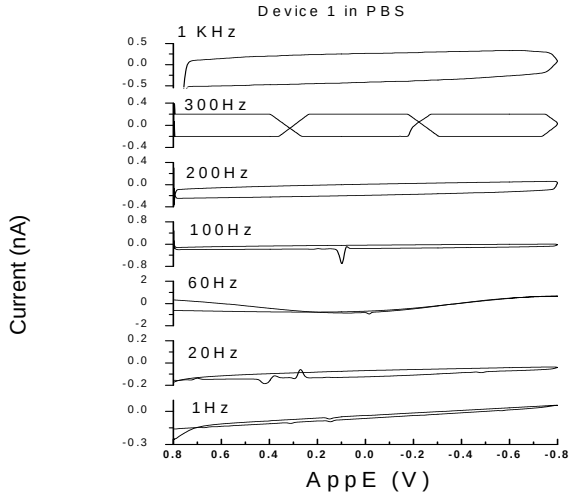

Fig. 4A. Depicts the i-V curve profiles in PBS control solution with scan rate change from 1 Hz to 1 KHz. Shapiro steps can be seen.

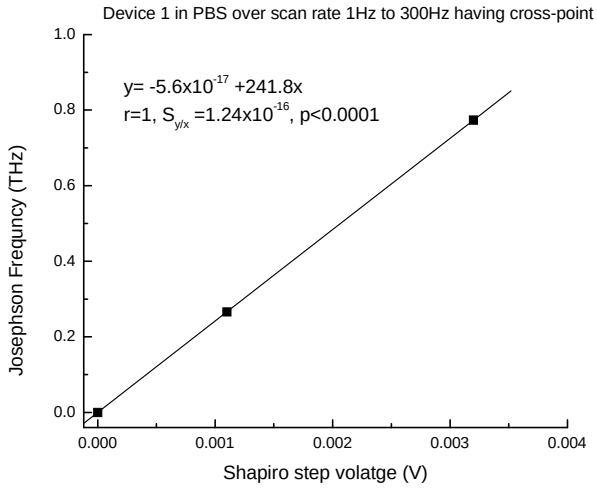

Fig. 4B. Depicts the plot of Josephson frequency vs. Shapiro step voltage over scan arte 1, 60 to 300 Hz that have cross-points of FFTJJ.

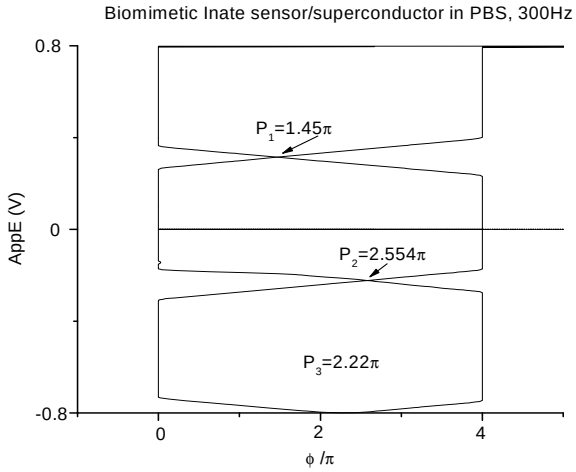

Fig. 4C. Depicts the phase change of Device 1 in PBS solution with scan rate 300 Hz.

3.2. Sensing of Biological Substances

Circular current induced by junctions of aromatic molecules of the delocalized molecules has drawn interest from theoretical scientists [26-27]. Scientists have envisioned its future applications. E. Chen's group identified and evaluated the circular current presented in an organic memristor/memcapacitor device when applied to a dc potential on the half memcapacitor cells for 10 cycle scans using the cyclic voltammetry (CV) method at a fixed scan rate 20 mV/s in 1 M methanol solution without any other reagent. The exponential increase of the current indicates its Schottky diode behavior, i.e., a small potential drop at 0.1 V from the origin and then increased nonlinearly that provides higher switching speed and system efficiency [28]. Delocalized electron relay through the multiple residue groups, hydrogen bounding and hydrophobic π-π staking, could be the driving force [28]. The heterogeneous surface controlled Direct Electron Transfer (DET) process in terms of DET Constant *Ks* was calculated according to E. Laviron's method at 107/s, and the diode peak is 192.5/s, and it may reach 220.2/s from the vector contributions from our calculation [29-33]. The vortex force of the circular current laid a

foundation to induce a non ferromagnetic field from low frequency to high frequency by turning different angles of the memristive/memcapacitive energy storage device, and it reduced operational energy by 33 % [34]. Further, our group discovered the toroidal array nanostructured memristive/memcapacitive device also can act as a neuronal memory device having both memory and energy storage functions with extended memory time at a reentrant neuronal circuitry with higher reentrant energy sensitivity of 0.12 *pj/bit/s/*μm^3 without Aβ compared with Aβ, 13 *aj/bit/s/*μm^3/nM over Aβ 3.8-471 nM range over 0.003-4s [35-38]. In the present report, we could not utilize the DET phenomenon in the innate MMP-2 device in PBS solution, not even any other memristive driving force, because no active peaks exist in the CV curves shown in Fig. 4A, except the FFTJJ vortices asymmetric braiding observed. A hypothesis was raised that the asymmetric braiding might be useful as a powerful driving force to initiate a DER for sensitive detection of biological substances if more suitable barriers present, because Fig. 4A showed there is a bidirectional phase change asymmetrically in the PBS solution accompanied with ± 0.2 nA super current at zero-bias under external magnetic field = 0, which indicates a potential power can be used. The FFTJJ repeatability curves on different days conducted with 6 consecutive scans at 300 Hz were also obtained (data are not shown here).

The results demonstrated the DET_{ox} peak and the MEM peak current intensity had exponentially increased in the presence of 5 fg/mL collegan-1 by 185,000-fold and 220,000-fold at the first scan cycle compared with the PBS control at 300 Hz scan rate, and the intensity continued to increase until, at the fifth cycle, it reached 500,000-fold and 495,000-fold for DET_{ox} peak and the MEM peak, respectively as shown in Fig. 5A. This drastic event proves the FFTJJ vortex's driving power enabled collagen-1, acting as an analyte and as a dielectric insulator barrier, made the DET peaks occur and in return the vortex amplified itself as shown in the curves, (1) a memristive characteristic point occurred with the hysteresis point at zero bias with the current is zero; (2) the vortex penetrated the insulating layer in a spontaneous way; (3) the exponential first order rate of the DET_{ox} signal increase vs. scan time of the 10 consecutive cycles through the bidirectional direct electron-relay promoted by the d-wave is 0.046/s, which is a little larger than the rate of 0.041/s by the MEM peak, as shown in Fig. 5B.

When collagen concentration increased to 150 ng/mL, the signal intensity of MEM peak inversely reduced as seen in Fig. 5C. An inverse linear relationship between current and the collagen concentration was observed over 5 fg/mL to 150 ng/mL. The most important change of the i-V curve at 150 ng/mL was that the superconducting current increased at zero-bias by 22 to 90-fold compared with the control under the same experimental conditions; the voltage difference between the DET_{ox} peak and the MEM peak was 0.415 V compared 1.57 V with 5 fg/mL collagen, which indicates that collagen played a crucial constructive role in promoting memristivity and superconductivity. Collagen is the most abundant protein in the human body. It is the primary structural component of the extracellular matrix (ECM) that is responsible for physical maintenance of all cells [39]. A long history of the conventional approach has shown the denatured collagen acted as a substrate, either to probe collagen degradation or as a substrate to probe the matrix metalloproteinase (MMP) activity [40-41]. However, a clinically useful detection range at the low end for collagen-1 is difficult to accomplish due to the denaturing process. As the knowledge and understanding advanced in the JJ superconductor device, we were able to show the FFTJJ Effect could be used for biomedical sensing which was impossible before, due to the lack of the active peaks.

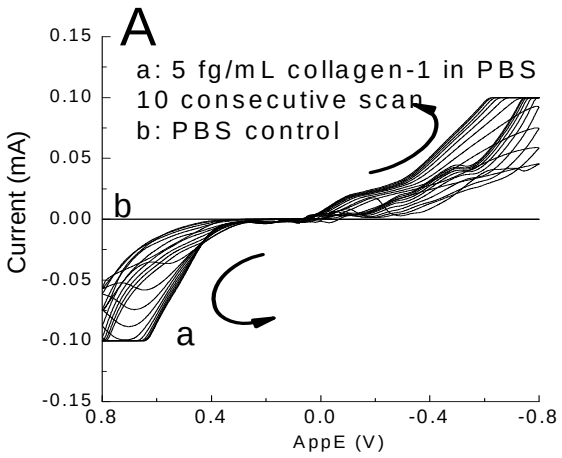

Fig. 5A. Depicts the i-V curve profiles with or without 5 fg/mL collagen-1 in PBS solution with 10 consecutive scan at 300 Hz using the innate superconductive/Mem-element device.

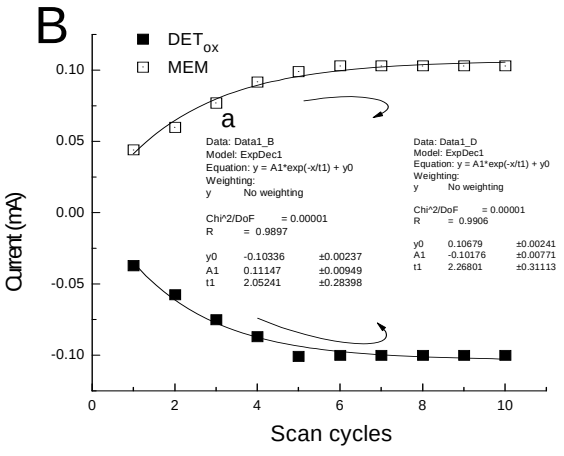

Fig. 5B. Depicts the trends of the DET peak and MEM peak current vs. scan cycles.

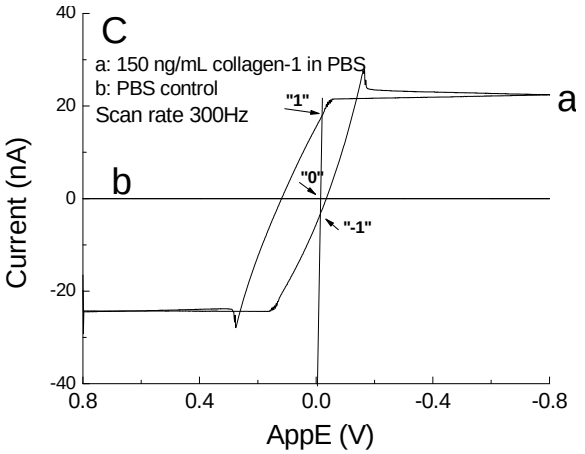

Fig. 5C. Depicts the i-V curve in the presence of 150 ng/mL collagen compared with the control.

4. The FFTJJ Dynamic Multiple-Variable Study Between Differentiate Conductivity, Inductive Energy and Charge Energy

Stern's group reported the observation of Majorana bound states of Josephson vortices in topological superconductors, and the equations of three types of energy contributions to the Josephson vortices in a long circular junction in a Sine-Gordon system was published [42]. The Josephson junction energy was from the Cooper pair, the magnetic energy was from the inductivity of the circular vortex, and the charge energy was from the SIS quantum capacitor-like device [42]. The vortex suppression of the super current effect also was considered in the equation. However, there was no further analysis of how each component energy contributes to the system superconductivity from the experimental data. Cosmic's group reported seeing the vortex in a Josephson array based on a fractional Josephson Effect in the vortex lattice [43]. The Hamiltonian of the Josephson Junction Array (JJA) was given in the combinations of the first part of charging energy obtained from all arrays and the second part of the Josephson Effect energy [43]. Still, no reports were given on how the energies impacted on one another in their experiment. Inspired by their experimental works, our attempt was, by using the 3D dynamic map method, to further seek a method to elucidate the reactions between the component energies to the superconductivity of the vortex array system at room temperature without external magnetic field applied. Our experimental data were shown on the i-V curves and the AFM structure of the superlattice array. The modified Sine-Gordon system energy for our d-wave vortex array is:

$$E^n_{JJA} = (½)C^{-1}{}_i(Q - en_{1...i})^2 \quad (1)$$

$$E^n_L = (½)\,\mu_0 N^2{}_{n=1..i}.A.L^{-1}{}_{n=1..i}.I^2{}_{n=1..i} \quad (2)$$

where E^n_{jjA} is the charge energy of Josephson Junction arrays at n = 1..i; Q is the charge, C is the total capacitance at n = 1..i, en is the n quantum particles at 1..i data point with an energy periodic in h/e for Josephson effect for d-wave [25]; E^n_L is the Inductive energy induced by the circular toroidal array. N is the turning umber around the toroidal porous at n =1..i, A is the cross-sectional area of the porous, L is the length of the wending, μ_0 is the magnetic permiability constant in free space; I is current. The toroidal arrays are in series connected.

4.1. The Multiple-Variable Study Between Potential, Current and Differentiate Conductivity

How variables like current and applied potential impact on the differential conductance, especially conductance at zero-bias, which is the superconductance at the ground energy state is an interesting topic using our experimental data obtained from the FFTJJ device. This study will lead us to further study of the relationship between inductive energy and charge energy impacts on superconductivity. The results of multiple-variable studies between differential superconductance, current and potential were presented in the 3D raw data dynamic map, the contour maps with different conductance ranges fitting in PBS control solution in the FFTJJ device shown as control maps in Fig. 6A, Fig 6B and Fig. 6C, respectively, compared with that in the presence of 150 ng/mL collagen in Fig 6D, Fig. 6E and Fig. 6F under 300 Hz scan rate, respectively. By comparing Fig. 6A and Fig. 6D, the results shown at the forward scan at ± 1Δ (±1 mV), the negative supercurrent is 28.45-27.0-fold higher with collagen than with the control; the control has same current value of -0.2 nA at ±1 mV, but with collagen, it has supercurrent of -5.7 and -5.39 nA, hence, the superconductance produced was -1137-fold and +1077.3-fold higher compared with the control at 1 mV and -1 mV, respectively; at zero-bias potential, the supercurrent is -5.54 nA compared with the control of -0.2 nA, and the quantum differential conductance has infinity value and without energy dissipation. It was noticed that the amplification of the superconductivity by the presence of collagen was based on the initiation of the fractional Josephson effect in the control sample, and due to the phase change at 1.45π (at 0.34 V) and 2.554π (at -0.19 V), both hysteresis pinches were located in the Fermi zero energy surface, rather than the conventional fractional Josephson effect of the pinch of 0 and π phase change located at zero-bias [44]. However, we observed in the Fermi zero energy surface, at the ± 1Δ, there are two excited superconductance peaks caused by the two phase irregular braiding. There is an inversely linear correlation between the intensity of the differential

conductance and the applied potential, i.e., as the potential increases, the conductance decreased forming a near 45° diagonal line, which implied the energy is inversely proportional to a half of the capacitance when current increased, evidenced by observing that at the location of zero-bias, there are highest magnetic flux lines penetrating so that the vortex suppressed the Josephson current as shown in Fig. 6B. Further, there were six vortices from current 0.2 to 0.7 nA; the vortices' shapes and phases were changed with current changes, which indicates the fractional vortex presences as shown in Fig. 6B and 6C. The irregular shaped vortex was seen at zero-bias indicating that is a fractional vortex. The difference between Fig. 6B and 6C was shown by the intensity of the superconductivity change in the contour map view, with one being near the Fermi purple surface (Fig. 6C) as opposed to the one far from the Fermi surface (FIG. 6B). In Fig. 6C, the supercurrent is observed from negative to positive (-0.2 nA to 0.2 nA) at zero-bias potential, and the negative superconductive vortices are observed oscillating across the Fermi surface with the positive superconductive vortex together; in contrast, from a far distance of Z direction view, no oscillation could be seen in Fig. 6B. By comparison with Fig. 6E and 6F, the strength of positive quantum conductance at zero-bias from - 5.5 nA to 15 nA, appeared regardless, whether in the far or near Z-directional view. Collagen's contribution to the quantum conductance was its ability to turn a fractional phase braiding surface in the i-V curve over ± 0.25 nA in the control to a $\pi/2$ angle, so the 2 pinch points' spatial locations were covered bias = 0, -5.4 nA; and bias=0, 15.41 nA, plus at ± 1 mV at -5.39 nA and 15.4 nA, respectively, we were unable to see the negative quantum conductance at the pinch points, because the z-direction view was too close to the Fermi surface and the magnetic flux was so strong.

4.2. Multiple-Variable Study between Differentiate Conductivity, Inductive Energy and Charge Energy

Comparing Fig. 7A with Fig. 7D between the control and in the presence of collagen, we found that per unit inductive energy contributing to the superconductance at ± 1Δ in the forward scan was 35,000-fold and 37,404-fold higher with collagen than without collagen; For the backward scan, at the same ± 1Δ, per unit inductive energy contribution to quantum conductance was 12687-fold and 9.9×10^6-fold higher with collagen than without. In the case of control, for three out of four situations in forward and backward scans, there was 769-fold higher contribution from inductive energy than from the charge energy. Fig. 7B shows there was a diagonal rectangle zero conductance area connected; the inductive energy has positive contributions to the quantum conductance at the left-hand corner with an inductive energy of 0-50 pJ/cm^2 and charge energy from -1 to -5 nJ/cm^2 as shown in Fig. 7B at a close Z-direction surface view compared with a far Z-direction surface view of Fig. 7C, in which the background shows more negative conductance than Fig. 7B where the small positive conductance square at the left-hand showed less magnetic flux penetrating in Fig. 7C.

Fig. 7E and Fig. 7F are the contour maps with a far Z-directional surface view and a near surface view in the presence of collagen, respectively. The highest positive oscillation quantum conductance pitch was located at inductive energy 0.199 pJ/cm^2 and charge energy 0.002 μJ/cm^2 at 1 mV with the conductance value of 616 μS/cm^2 from the backward scan, while another oscillation center with the quantum conductance pitch was observed at x=0.202 pJ/cm^2, y= -1.98 μJ/cm^2 at V=0 with infinite conductance causing bidirectional resonance, and the highest negative conductance was at x=0.205 pJ/cm^2, y=-2.0 at -1 mV with the quantum conductance -625.5 μS/cm^2. The total area covered by the positive conductance vs. total area of negative conductance is 1:2. In a near surface view in Fig. 7F, there was no oscillation center observed in the negative conductance area in which the center is a hole, while the positive conductance pitches are greater with the magnetic resonance between the center pitch and the small pitch from x=0 to 0.05, where y= -0.25, indicates the fractional vortex dynamic behavior in the tunnel. The results provided important evidence that at the FFTJJ, the circulating array current induced magnetic energy is dominant over the total charge energy contributed to the quantum conductance in the FFTJJ barrier. In the presence of collagen, it exponentially increased per unit inductive energy contribution to the quantum conductance over the charge energy contribution, which indicates the FFTJJ array is a non-linear inductor array.

5. Activated Biomimetic MMP-2 Device Also Actives Superconductivity in the Presence of Collagen

5.1. In the Presence of Collagen in the MCD Media

Collagen is the most abundant protein in the human body. It is the primary structural component of the extracellular matrix (ECM) that is responsible for the physical maintenance of all cells [39]. The triple-helical structure of collagen assembles into insoluble collagen fibrils to strengthen the structural integrity of bones and tissues therefore preventing normal proteinase from engaging [39, 45].

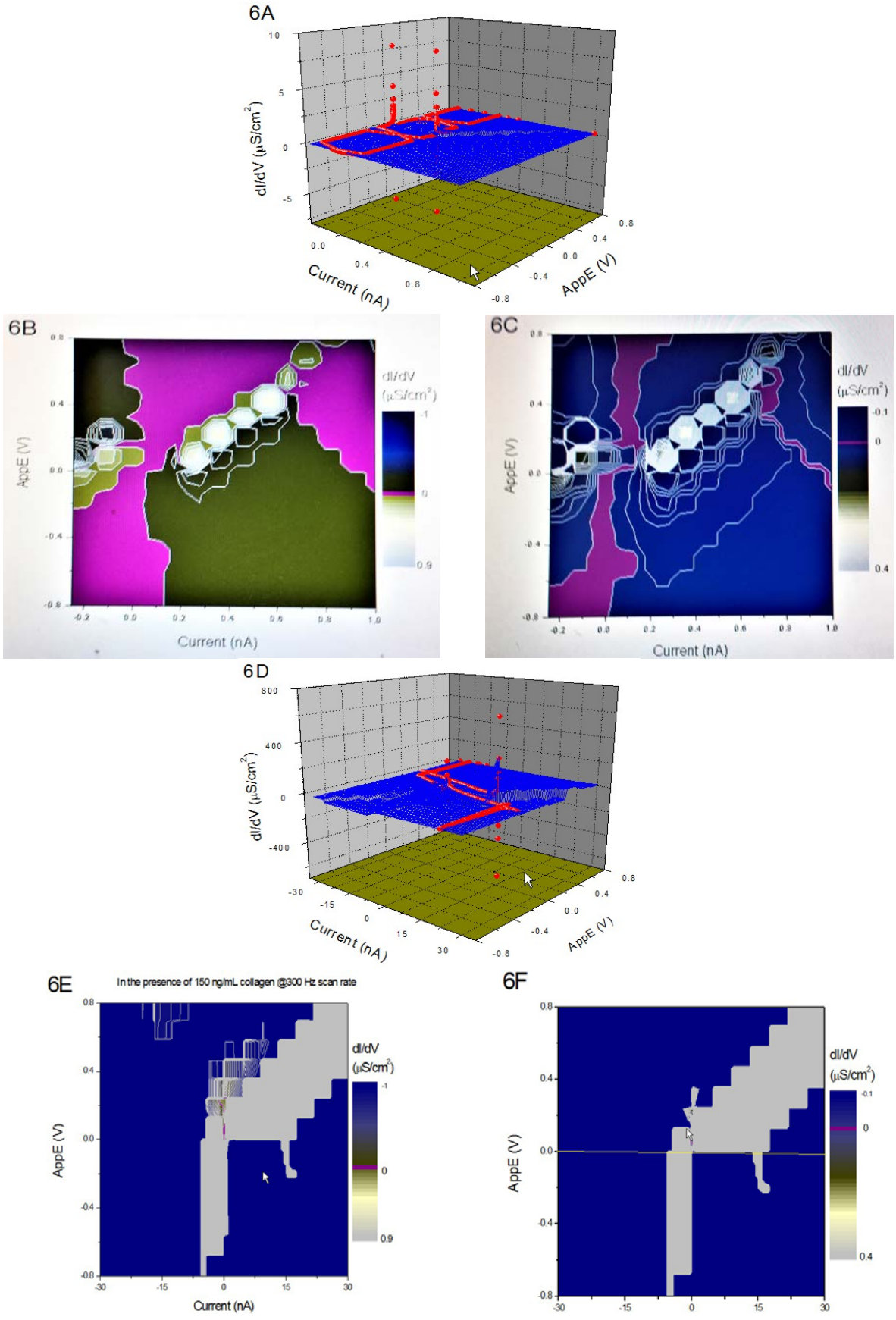

Fig. 6A, 6B and 6C. Maps of multiple-variable relationship between **differential superconductance**, **current and potential** in the 3D raw data dynamic map, the contour maps with different conductance ranges fitting in PBS control solution in the FFTJJ device shown as control maps under scan rate 300Hz. **Fig. 6D, 6E and 6F.** Maps in the presence of 150 ng/mL collagen.

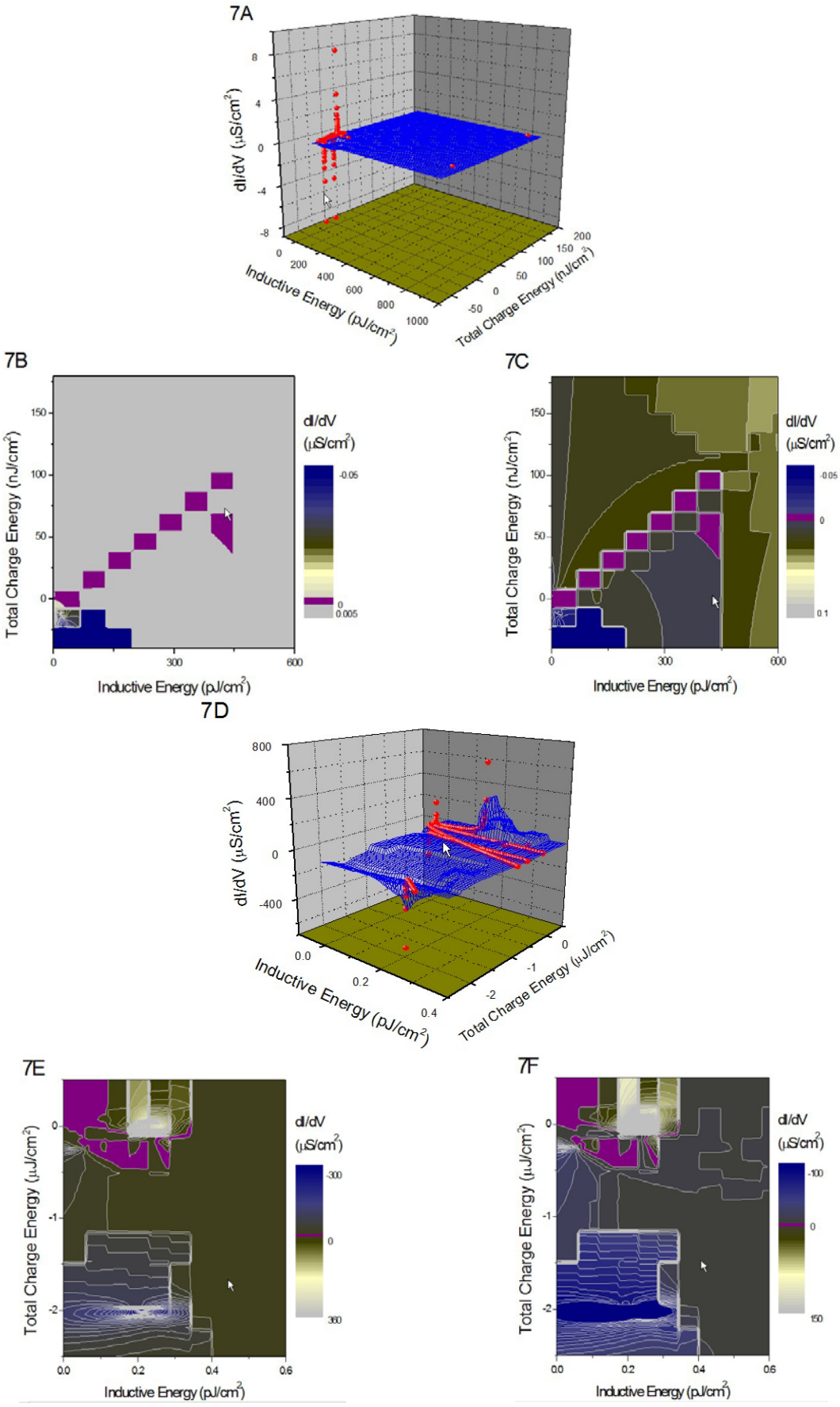

Fig. 7A, 7B and 7C. Maps of multiple-variable relationship between **differential conductance, inductive energy and charge energy** in the 3D raw data dynamic map, the contour maps with different conductance ranges fitting in PBS control solution in the FFTJJ device shown as control maps under scan rate 300Hz. **Fig. 7D, 7E and 7F.** Maps in the presence of 150 ng/mL collagen.

Collagen is a double edged sword, not only actively paving the road for physiological normal cell and pathological abnormal cell adhesion, migration and intracellular communication, but also activating some receptors for either over-production or failure of matrix degradation caused by either bacterial collagenase or abnormal fibrosis from fibroblast cell, endothelial cell or epithelial cells; hence many diseases are associated with the malfunction of collagen [44-47] A conventional approach which has been used for a long history is to denature collagen by means of heating in order to eliminate the cysteine group and use collagen as a substrate to probe collagen degradation or to study matrix metalloproteinase (MMP) activity [40, 48-49]. Our prior work shown, by using a non-denatured protein MMP-2 device and using the biomimetic MMP-2 device, both could direct detect extremely low collagen-1 concentration due to the Josephson toroidal junction approach and the organo-metal superlattice membranes [16-17]. This section will emphasize and confirm that after denatured the biomimetic "innate MMP-2" device, the energy band occurred and the Cooper pairs penetrated the FFTJJ barrier. Fig. 8A demonstrates different media effects on the supercurrent on the activated biomimetic MMP-2 device in the presence of 50 ng/mL collagen with 50 ng/mL MCD and compares 50 ng/mL collagen without MCD and with pure MCD and PBS control, respectively. Two supercurrents were observed and labeled as P_1(0V, -0.049A) and P_2(0V, 0.10A) at zero-bias, shown in Fig. 8A. This increased 3571-fold current intensity with collagen in MCD media over that of collagen alone (shown in the insert). Fig. 8B demonstrates that the activated biomimetic MMP-2 device having a quantized conductance intensity of 7344.6-fold higher in collagen with MCD than the collagen alone, MCD promoted the Direct Electron-Transfer (DET) and formed long range delocalized DER, as shown in the DER mechanism model in Fig. 8F. The 50 ng/mL MCD control alone showed a small 4.8 μA background current in PBS. The significant increase of the superconductivity in the presence of collagen and MCD indicates a proposed mechanism model shown in Fig. 8F. It was shown in our prior work that the well-aligned cyclodextrin truncated donut-like cavities formed large nanopore toroidal wells with dipole polarized circular current flow in opposite directions induced a non-ferromagnetic field [33-34]. Fig. 8C depicts an enlarged view of the zero-bias superconducting peak in the forward scan and another supercurrent 0.1A at zero-bias at back scan in the presence of 50 ng/mL collagen with 50 ng/mL MCD. Fig. 8D depicts a 3D Cooper Pair's dynamic tunneling and crossing the FFTJJ barrier. Fig. 8E depicts the image of the superconducting bands at zero bias ± 1Δ and sub bands. Fig. 8F depicts the biomimetic MMP-2 model and the "Zinc Finger" for promoting DER effect. The MCD is a crucial element for forming the "Zinc Finger" with a CD cavity protection shield on it, so it protects the delicate DER effect from being broken when denaturing protein of cystein occurs that may cause conformation and polarity change. Knowing that a natural zinc finger used conventionally for repairing DNAs, does not have the CD protective "glove", therefore our approach may offer a benefit when used for direct cleavage of proteins and repair of DNAs without using other "Third Party" means.

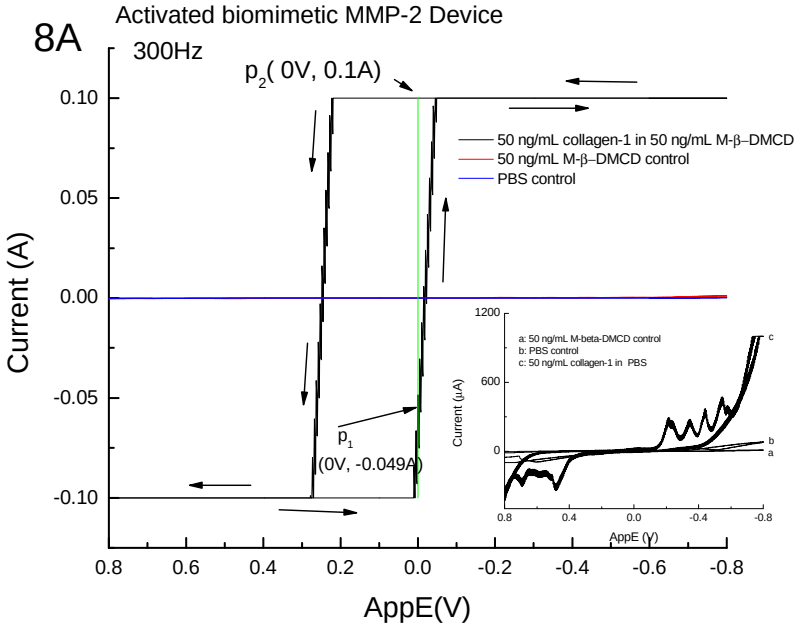

Fig. 8A. Depicts denatured Device i-V curve in the presence of 50 ng/mL collagen-1 with 50 ng/mL MCD in PBS compared with the MCD control and the PBS control respectively. Insert is the curve with 50 ng/mL collagen-1 alone compared with the curve of MCD control and PBS controls after activated the device.

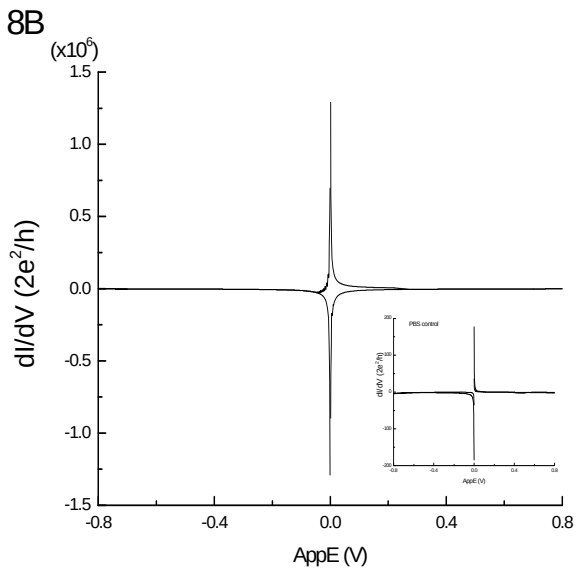

Fig. 8B. Depicts the quantum dI/dV curve compared with the curve of collagen alone in the insert.

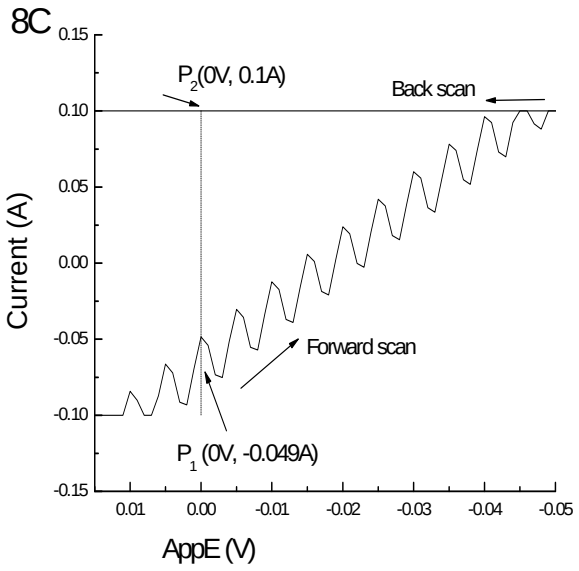

Fig. 8C. Depicts the enlarged view of zero-bias superconducting peak in the presence of 50 ng/mL collagen and 50 ng/mL MCD in PBS as shown in Fig. 8A.

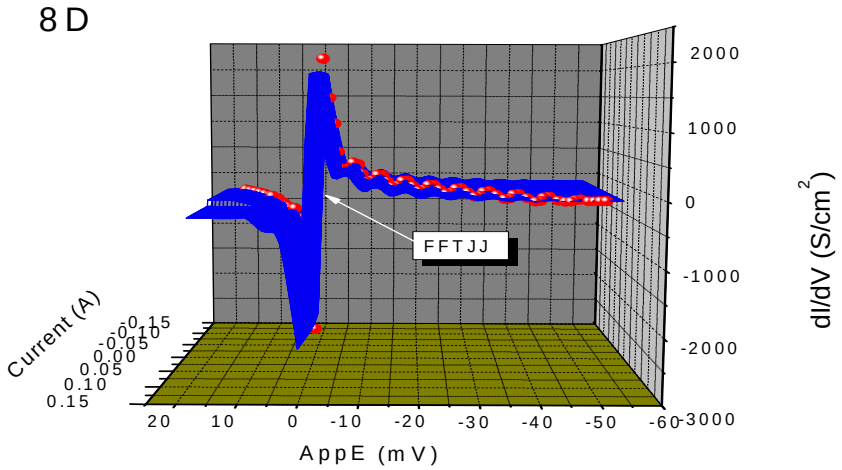

Fig. 8D. Depicts a 3D Cooper Pair's dynamic tunneling and crossing the FFTJJ barrier.

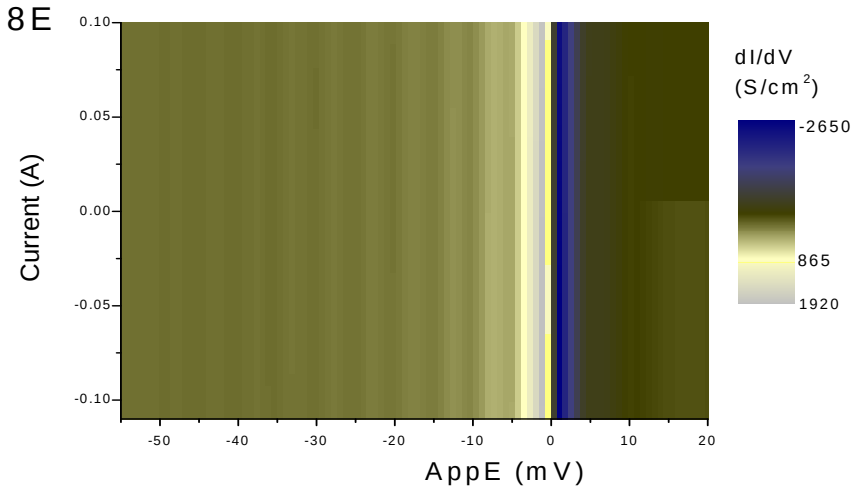

Fig. 8E. Depicts the image of the superconducting bands at zero bias ± 1Δ and sub bands.

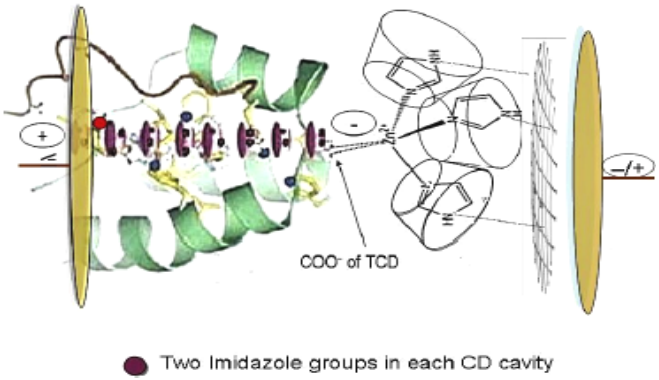

Fig. 8F. Is an art model for the delocalized DER system with the red ball represents the sulfur atom of cyctein, and purple balls are imidazols in the CD cavity, and the zinc atom with three MCDs represents the "Zinc Finger"; the collagen lattice is in the right-hand side forming weak links with the zinc finger. The electrodes are switchable connected gold chips.

5.2. The Analytical Performance

In this Section we present the results of the impacts of collagen concentration change on the analytical performance of the activated biomimetic device using the cyclic voltammetry (CV) method. Our recent publications using the innate superconductive/Mem-element device to detect collagen using human serum, whole blood specimens evaluated by the CV method, the voltage method and the Chronoamperometric method (CA) were in the literature [16-17]. Fig. 9A depicts the i-V curves in the various collagen concentration from 50 fg/mL to 200 ng/mL in 5 levels compared with the PBS control at 300 Hz scan rate. We found both the DET_{ox} and DET_{red} peak intensity increased as the concentration increased. At the 200 ng/mL concentration**,** there is a phase change from horizontal curve line to a $\pi/2$ vertical change at zero-bias, which confirmed our observation reported in Section 3.2, in the presence of 150 ng/mL collagen using the innate Biomimetic MMP-2 device. Fig. 9B demonstrates the exponential current increase curve of the DET_{red} peak intensity vs. collagen concentration over collagen concentration of 0.0, 50 fg/mL, 500 fg/mL, 500 pg/mL and 50 ng/mL in 5 levels. The linear range up to 500 pg/mL has a sensitivity of 230 μA/(ng/mL).

6. Quantum Computing

6.1. Quantum Computing with Mem-element Characteristics

Current DC or RF Superconducting Quantum Interference Devices (SQUID) made faster switch time; however hundreds of MHz electromagnetic field applied onto a tank circuit coupled to the SQUID is needed for the system to work under cryogenic conditions [50-52]. As a consequence, superconductor qubits are vulnerable to low frequency noise with sources coming from 1/f noise, wave dephasing noise, flux noise, critical current noise, quasiparticle tunneling noise and capacitance noise [51, 6]. The Josephson junction is a key element in the broader area of superconductivity devices including the SQUIDs [21, 50-52]. The nature of the qubits operating multiple states at the same time is more sensitive to decoherence caused by the control and readout circuitry and the environmental noise as well as the qubits own intrinsic low frequency noise, than conventional computing [51, 6]. Nevertheless, so far, that superconductive material made qubits of dc SQUID or rf SQUID has not demonstrated its function as a memory cell; i.e., a device remembers the past events; hence, SQUID device has to be connected with memory devices and other auxiliary devices in order to be a large scale quantum processor for computational function. Our FFTJJ qubit device offers three states in the quantum computing: at "1" state with the spatial location at (0 mV, 0.59 μA) and "-1" state with location at (0 mV, -0.69 μA), and the "0" state window is located from (0 mV, 0 μA) to (-1 mV, 0 μA), respectively, as shown in Fig 9C**.** This origin point contained in the rectangle loop of the i-V curve is the signature feature of a "O-type" loop memcapacitor whose hysteresis pinch point does not directly pass origin. The loop contains origin, because the permeability of the materials cannot instantaneously follow the current (flux) across the inductor because of a negative charge or negative capacitance [52]. These "O-type" memdevices have memory of the past event. In that observation, the "0", "1" and "-1" states simultaneously occurred with its Shapiro step of 3 mV shown in Fig. 9D with a switch time of 1.4 ns. There was no energy loss for the operations at these states. Similar observations also confirmed the quantum computing capability with the innate device shown in Fig. 5C in the presence of 150 ng/mL collagen. In comparison, Fig. 5C shows the quantum computing at "0" state, "1" or "-1" state as (0, 0) contained inside the vertical loops, (0 mV, 15.5 nA) and (0 mV, -5.5 nA), respectively. The i-V curve has a Shapiro step of 1 mV.

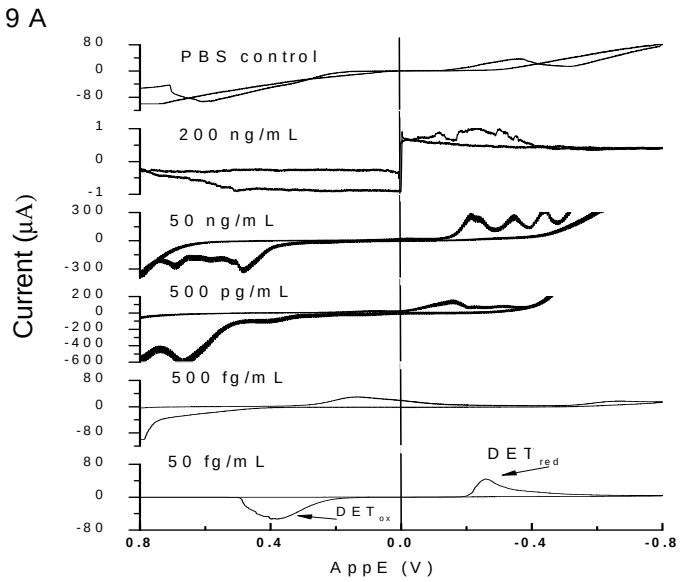

Fig. 9A. Depicts the collagen concentration impact on the i-V curve profiles over concentrations from 50 fg/mL to 200 ng/mL in PBS solutions compared with the control with the denatured qubit Device.

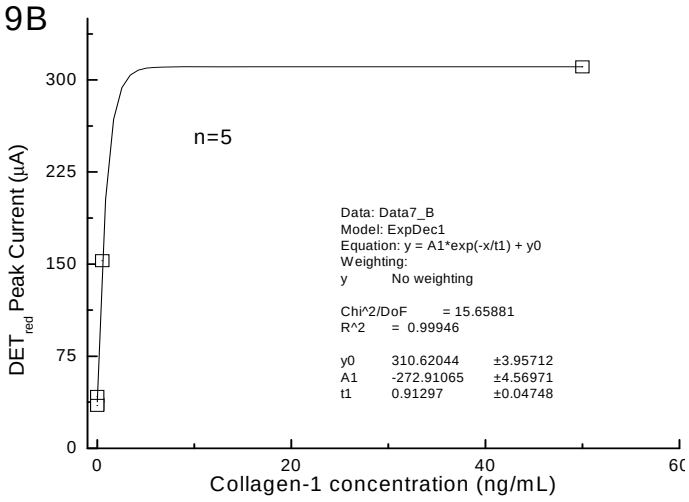

Fig. 9B. Depicts the non-linear calibration plot.

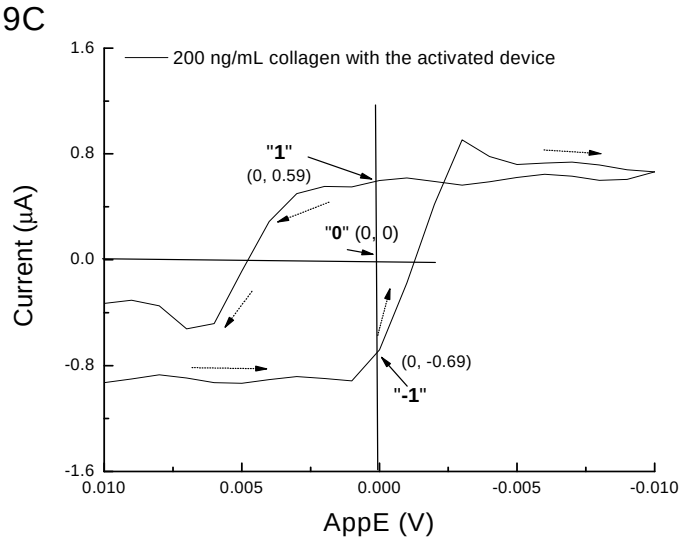

Fig. 9C. Depicts the detail assignments for quantum computing "0", "1" and "-1" three states at zero-bias in the presence of 200 ng/mL collagen.

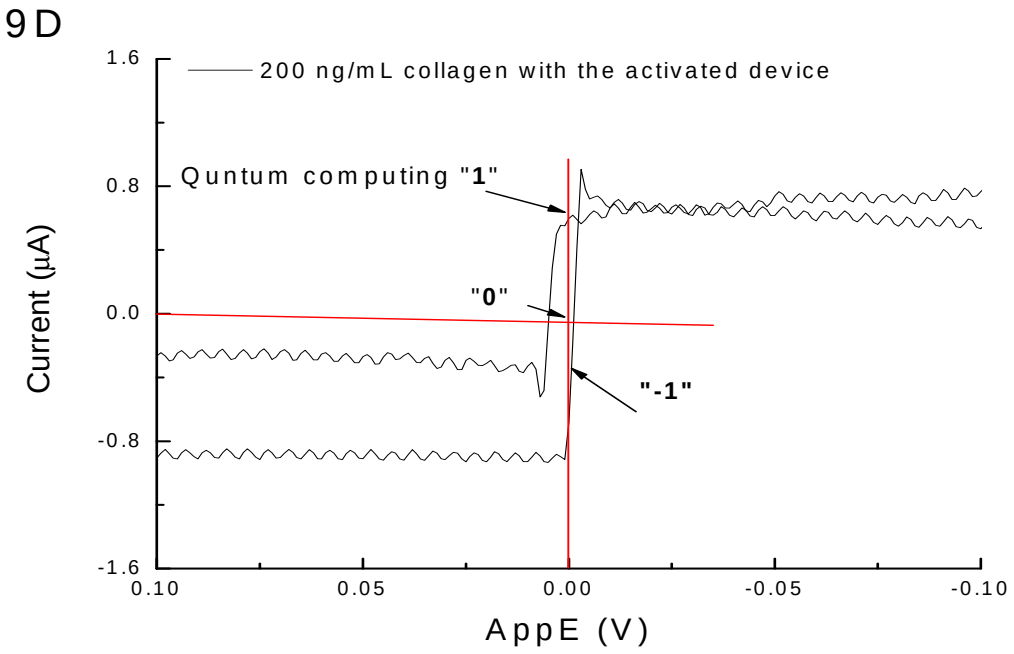

Fig. 9D. Depicts the Shapiro steps occur in the i-V curve.

6.2. Quantum Computing Without Switch Time Delay

Using the CV method to define the quantum computing in "0" and "1" states at zero-bias, we can also define the "0" and "1" states at zero current by the voltage method. The Double Step Chronopotentiometry (DSCPO) method, i.e., the voltage method, was used to set up each of the two steps current =0, each step time period was set in one of the constant values, such as 1 ms. 4 ms, 40 ms to 800 ms under conditions (1) with 150 ng/mL collagen and (2) with 150 ng/mL collagen and 50 ng/mL MCD in PBS compared with the control as shown in Fig. 10 A, 10B, 10C to 10D. Curves with collagen in the MCD media have the highest voltage amplitude compared with collagen alone. Curves in the control have the lowest voltage intensity. We observed the phase changes between the curves in Fig. 10B, 10C and 10D compared with the phase of the control sample. The "0" value assigned at the curves with voltage = 0 and current = 0, the "1" assigned at voltage larger than 0 with current = 0; and "-1" can be seen at voltage less than 0 with current = 0. Fig. 10D shows that with superposition of the switch time over "0" and "1" states or "-1" state, there was no time delay at all compared with other Figures. It revealed that in the presence of collagen in the MCD media, it promoted DER and superconducting. Herein the switch time between states was reduced, which offered an advantage for solving the lagging switch time problems. The spontaneous discharged voltage pulses from the qubits device indicates there was an embedded power in the device which can self-power quantum computing in the presence of collagen without the need of a microwave power supply; nor does it consume any energy, as shown in Fig. 11 in the open circuit potential curve in the presence of 150 ng/mL collagen in PBS. The spontaneous first-order rate constant of the open circuit potential is 0.012 V/s.

7. Experimental

The FFTJJ Device 1 was freshly prepared by a self-assembly method with compositions of triacetyl-ß-cyclodextrin (TCD), polyethylene glycol diglycidyl ether (PEG), poly(4-vinylpyridine) (PVP), bis-substituted dimethyl-β-cyclodextrin (bM-β-DMCD), cysteine and embedded zinc chloride on gold chips with appropriate proportions at 37°C for 96 hours. The procedures were reported in reference [16]. The activated (denatured) biomimetic MMP-2 device was accomplished by heating the chip on 80.0°C for 5 minutes. After that the chip was washed thoroughly for 5 minutes with double distilled autoclaved, degassed and special filtrated water, and then put in the incubator for 2 hours at 37.0°C before use. Collagen-1 was purchased from Sigma (Atlanta, GA 30353). The mono imidazole substituted and bis-substituted dimethyl-β-cyclodextrin (mM--β-DMCD, or MCD and bM-β-DMCD) were synthesized, purified and characterized according to the literature [53].

The morphology of the AU/SAM was characterized using an Atomic Force Microscope (AFM) (model Dimension Edge AFM, Bruker, MA). Data was collected in TappingMode using silicon probes with 5-10 nm tip radius and ~300 kHz resonance frequency (Probe mode TESPA-V2, Bruker, MA).

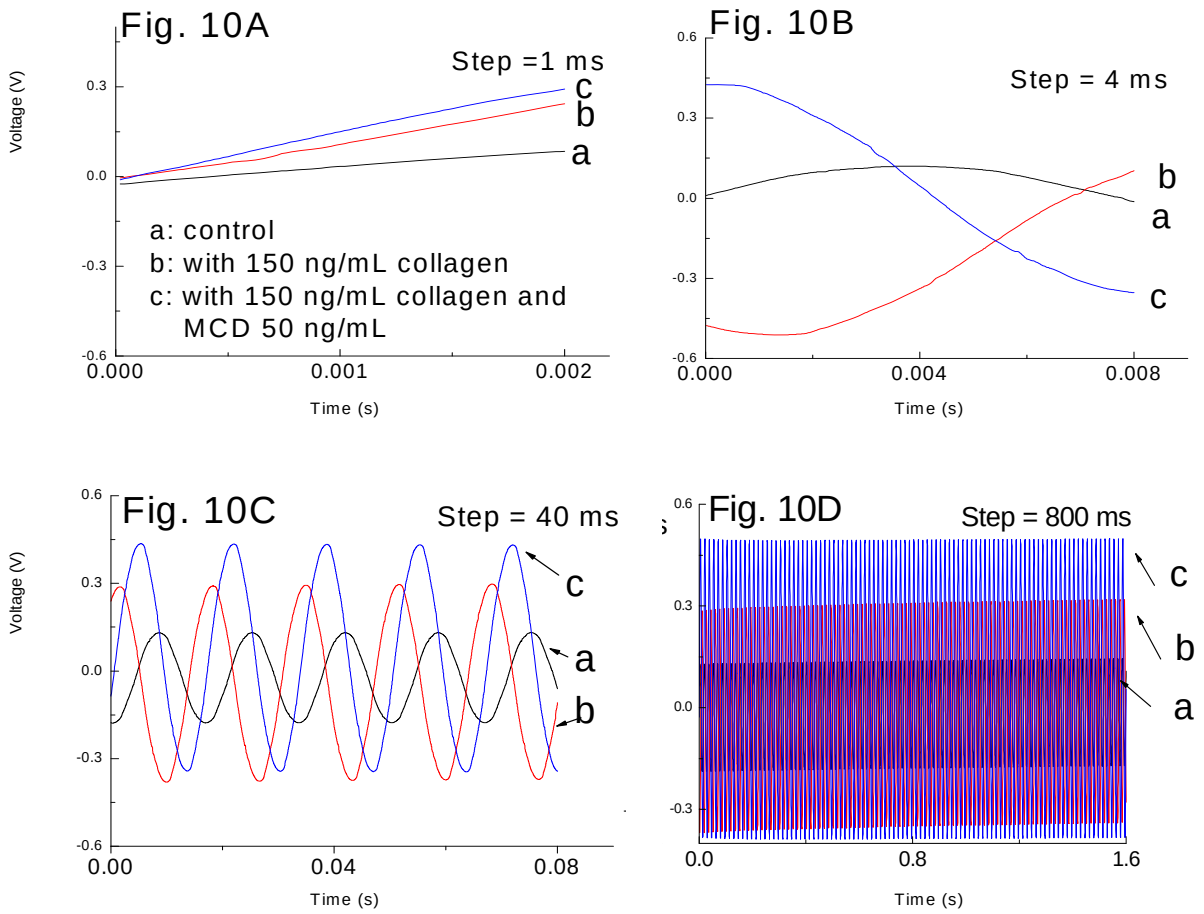

Fig. 10. Voltage vs. time curves at different step time using the DSCPO method for with 150 ng/mL collagen (b), with not only collagen, but also 50 ng/mL MCD (c) compared with the PBS control (a). For 1 ms step time was in **Fig. 10A**; 4ms, as in **Fig. 10B**, 40 ms time as in **Fig. 10C** and 800 ms time as in **Fig. 10D**.

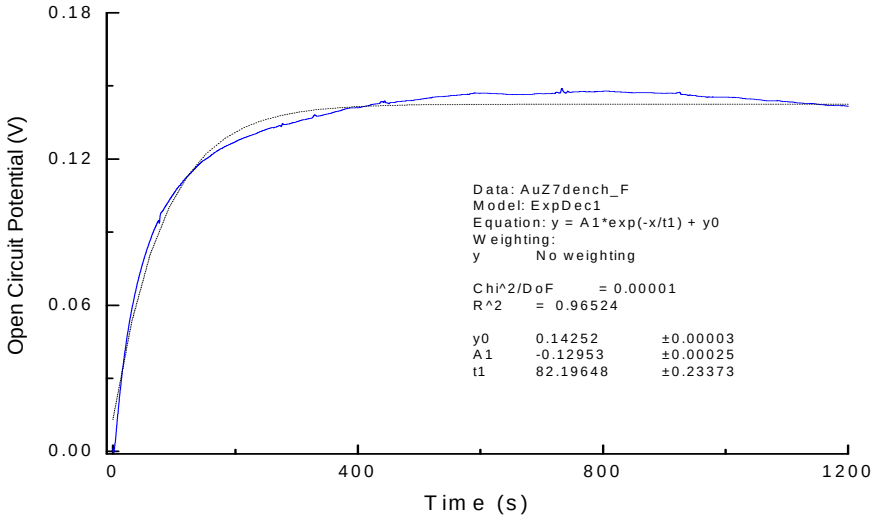

Fig. 11. Open circuit potential curve vs. time at current =0 in the presence of 150 ng/mL collagen in PBS solution.

8. Conclusions

Self-powered FFTJJ qubits devices for sensing, memory storage and quantum computing were demonstrated. The functions of the FFTJJ membrane initiated the intrinsic magnetic flux accompanied with Josephson fractional phase change that promoted the superconductive quantum computing function with sensing and memory storage in the presence of collagen as an analyte and an insulator. The slope value of Josephson Frequency vs. Josephson Shapiro step voltages over different scan

rates is a half of the Josephson Constant K_J. This indicates the fractional Josephson Effect occurred based on the Direct Electron-Relay (DER) vortices arrays observed at the first time. The FFTJJ dynamic multiple-variable study comparing differentiate conductivity, inductive energy and charge energy, presented in dynamic maps, enabled us to confirm that per unit of the inductive energy predominately contributed more to the superconductivity than per unit of the charge energy for the case with collagen and without collagen. The benefit of FFTJJ is its initiation of the intrinsic magnetic flux accompanied with unconventional phase change that paved the road for a more powerful superconductive quantum computing function with multiple types of sensing feasibility in the presence of collagen. The innate biomimetic MMP-2 sensor in the PBS solution showed no active DET peaks, nor any oxidation/reduction peaks. Only the fractional phase changes happened at 300 Hz, which proves the utility for promoting superconductive and quantum computing in the presence of collagen in the MCD media or in collagen alone. MCD itself does not have any active electrochemical peaks, but promoted the DER and enlarged the superconductivity.

The FFTJJ dynamic multiple-variable study comparing differentiate conductivity, inductive energy and charge energy with or without collagen has provided first hand experimental information for the first time under well controlled conditions in dynamic 3D maps and contour maps formatting. This enabled us to draw a conclusion regarding the quantitative contributions between the inductance energy and the charge energy to the superconductivity. This method provided evidence that the FFTJJ qubit device is an inductive energy dominant device for superconductive quantum computing. This technology may further help us to understand FFTJJ effect, and then it will broaden the applications in many areas to come.

Acknowledgements

We thank the NIST NanoLab for the clean room, the PDMS Lab and equipments used to fabricate the sensors. E. Chen thanks Dr. Richard Kasica's help and his valuable discussions. We thank Ms. A. Emerson for her editing of this manuscript.

References

[1]. University of Cambridge, Room temperature superconductivity: one step closer to the holy grail of physics, 9 July 2008, http://www.phys.org

[2]. A. Tantillo, Room-temp superconductors could be possible, Brookhaven National Laboratory, 29 September 2016, http://www.phys.org

[3]. M. Stone, "Holy Grail" of superconductors could revolutionize electronics, 18 August 2015, http://www.gizmodo.com

[4]. A. Nicodemo, What if superconductors could work at room temperature? 4 April 2018, news @Northeastern University.

[5]. K. K. Likharev, Dynamics of Josephson junctions and circuits, *Gordon and Breach Science Publishers,* New York, 1996.

[6]. A. M. Zagoskin, A. Chipouline, E. Il'ichev, *et al.*, Toroidal qubits: naturally-decoupled quiet artificial atoms, *Scientific Reports*, Vol. 5, 16934; Doi:101038/srep16934, 2015.

[7]. C-K. Chiu, S. Das Sarma, Fractional Josephson effect with and without Majorana zero modes, *Physical Review B*, accepted December 19, 2018.

[8]. Y. Tanaka, H. Yamamori, T. Yanagisawa, *et al*., Experimental formation of a fractional vortex in a superconducting bi-layer, *Physica C: Superconductivity and its applications*, Vol. 548, 2018, pp. 44-49.

[9]. U. Kienzle, J. M. Meckbach, K. Buckenmaier, *et al*., Spectroscopy of a fractional Josephson vortex molecule, *Physical Review B*, Vol 85, Issue 1, 2012, pp. 014521-014528.

[10]. X. Liu, X. Li, D.-L. Deng, *et al*., Majorana spintronics, *Physical Review B*, Vol 94, Issue 1, 2016, pp. 014511-014523.

[11]. Y.-H. Li, J. Song, J. Liu, *et. al*., Doubled Shapiro steps in a topological Josephson junction, *Physical Review B*, Vol 97, Issue 4, 2018, pp. 045423-045428.

[12]. V. J. Wiedenmann, Induced topological superconductivity in HgTe based nanostructures, Doctoral Thesis, *Universität Würzburg*, Wurzburg, 2017.

[13]. K. Le Calvez, Signatures of a 4 pi periodic Abdreev bound state in topological Josephson junctions. Mesoscopic Systems and Quantum Hall Effect, *Universite-Grenoble Alpes*, 2017.

[14]. E. Goldobin, D. Koelle, R. Kleiner, Ground states of one and two fractional vortices in long Josephson 0−κ junctions, *Phys. Rev. B,* 70, 2004, pp. 174519.

[15]. H.-T. Kim, Analysis of the diverging effective mass in $YaBa_2Cu_3O_{6+x}$ for high-Tc mechanism and pairing symmetry, *International Journal of Modern Physics B*, Vol. 32, Issue 17, 2018, pp.1840031-1 to 1840031-11.

[16]. E. T. Chen, J. T. Thornton, P. T. Kissinger, S.-H. Duh, Nanobiomimetic Structured Superconductive/ Memristive Organo-Metal Devices at Room Temperature Serve as Amperometric Sensors for sub fg/mL Collagen-1, *Biotech, Biomaterials and Biomedical: TechConnect Briefs,* 2018, pp. 107-110.

[17]. E. T. Chen, J. T. Thornton, P. T. Kissinger, S.-H. Duh, Discovering of Collagen-1's Role in Producing Superconducting Current in Nanobiomimetic Superlattice Structured Organometallic Devices at Room Temperature Enabled Direct Quantitation of Sub pg/mL Collagen-1, *Informatics, Electronics and Microsystems: TechConnect Briefs,* 2018, pp. 43-46.

[18]. http://en.wikipedia.org/fractional_vortices.

[19]. K. Le Calvez, Signature of a 4 pi periodic Andreev bound state in topological Josephson junction, Dissertation, Universite Grenoble press, 2017.

[20]. M. Ternes, M. Pivetta, F. Patthey, W.-D. Schneider, Creation, electronic properties, disorder, and melting of two-dimensional surface-state-mediated adatom superlattices, *Progress in Surface Science,* Vol. 85, Issue 1-4, 2010, pp. 1-27.

[21]. D. Drung, J. Beyer, Applications in superconducting quantum interference devices SQUIDs (Chapter 8, pp. 245-316), Editors E. Wolf, G. Arnold,

M. Gurvitch and J. Zasadzinski, Preface, Josephson Junctions, History, Devices, and Applications, *Pan Stanford Publishing* Pte, Ltd, 2017.

[22]. I. Askerzade A. Bozbey, M. Canturk, Modern aspects of Josephson dynamics and superconductivities electronics, *Springer,* Chapter 2.3, 2017, pp. 69-79.

[23]. https://Physics.nist.gov/cgi-bin/cuu/value/kjos. The NIST reference on Constants, Units and Uncertainty.

[24]. C. A. Hamilton, C. Burroughs, K. Chieh, Operation of NIST Josephson Array voltage standards, *Journal of Research of the NIST*, Vol. 95, Issue 3, 1990, pp. 219-235.

[25]. F. Loder, A. P. Kampf, T. Kopp, *et al*., Magnetic flux periodicity of h/e in superconducting loops, *Nature Physics,* Vol. 4, 2008, pp. 112-115.

[26]. R. Islas, T. Heine, G. Merino, The Induced Magnetic Field, *Accounts of Chemical Research*, Vol. 45, Issue 2, 2012, pp. 215-228.

[27]. Idea Diode, http:en.wikipedia.org

[28]. E. T. Chen, J. T. Thornton, C. Ngatchou, S.-H. Duh, Nanostructured memristor sensor mimics acetylcholinesterase (ACHE) active sites in the gorge for fM detection of acetylcholine, *NSTi-Nanotech*, Vol. 2, 2014, pp. 200-203.

[29]. E. Laviron, General expression of the linear potential sweep voltammogram in the case of diffusionless electrochemical systems, *J. Electroanal Chem.,* Vol. 101, Issue 1, 1979, pp. 19-28.

[30]. E. T. Chen, J. Thornton, C. Ngatchou, S.-H. Duh, P. T. Kissinger, Study of the correlations between direct electron transfer rate constants and the effectiveness of cancer inhibitors using nanobiomimetic sensors, *NSTi-Nanotech,* Vol. 3, 2013, pp. 115-118.

[31]. E. T. Chen, Nanostructured biomimetic-enzyme sensing and energy storage, First volume, Third Edition, Editor S. E. Lyshevski, in Dekker Encyclopedia of Nanoscience and Nanotechnology, *CRC*, March 20, 2014.

[32]. E. T. Chen, C. Ngatchou, An electron-relay prototype supercapacitor mimics electrophorus electricus's reversible membrane potential for a high rate discharge pulse, *Sensors & Transducers*, Vol. 15, Special Issue, 2012, pp. 42-48.

[33]. E. T. Chen, Nanostructured Biomimetic Sensing and Energy Storage: Organic Memristor/Memcapacitors, Dekker Encyclopedia of Nanoscience and Nanotechnology, 3rd Edition, *CRC Press*, 18 January 2017. http://www.crcnetbase.com

[34]. E. T. Chen, Nanostructured organic memristor/memcapacitorof making with an embedded low-to-high frequency switch and a method of inducing an electromagnetic field, US Patent No. 9, 793,503, October 17, 2017.

[35]. E. T. Chen, J. Thornton, Jr. C. Mulchi, Nanobiomimetic Memcapacitor Memory Devices Identify Circadian Rhythm Dysfunction and Predict Early Signs of "Epilepsy" Using Reentrant Energy-Sensory Images, *Advanced Manufacturing, Electronics and Microsystems: TechConnect Briefs 2015*, 2015, pp. 200-203.

[36]. J. T. Thornton, Jr. C. Mulchi, P. T. Kissinger, E. T. Chen, Acetylcholine Repairs the Amyloid-beta Damage on Brain Circuitry and Memory Loss From a "Mutated Biomimetic Acetylcholinesterase" Neuronal Memcapacitor During Slow-Wave Sleeping, *Advanced Manufacturing, Electronics and Microsystems: TechConnect Briefs 2015*, 2015, pp. 226-229.

[37]. E. T. Chen, J. T. Thornton, Jr. C. Mulchi, Early Forming a Hummingbird-like Hovering Neural Network Circuitry Pattern with Reentrant Spatiotemporal Energy-Sensory Orientation Privileged to Avoid "Epilepsy" Based on a Biomimetic Acetylcholinesterase Memcapacitor Prosthesis, *Sensors & Transducer,* Vol. 191, Issue 8, August 2015, pp. 84-99.

[38]. J. T. Thornton, Jr. C. Mulchi, P.T. Kissinger, E. T. Chen, In Vitro Restoration of an amyloid-beta altered network circuitry in a 'mutated biomimetic acetylcholinesterase' memristor/memcapacitor neural prosthesis, *Sensors & Transducer,* Vol. 191, Issue 8, August 2015, pp. 100-113.

[39]. J. K. Kular, S. Basu, R. I. Sharma, The extracellular matrix: structure, composition, age-related differences, tools for analysis and applications for tissue engineering, *J. Tissue Engineering* Vol. 5, 2014, pp. 1-17.

[40]. B. H. San, Y. Li, E. B. Tarbet, S. M. Yu, Nanoparticle Assembly and Gelatin Binding Mediated by Triple Helical Collagen Mimetic Peptide, *ACS Applied Materials and Interfaces*, Vol. 8, 2016, pp. 19907-19915.

[41]. E. Seo, K. W. Seo, J.-E. Gil, Y.-R. Ha, *et al*., Biophysiochemical properties of endothelial cells cultured on bio-inspired collagen films, *MioMed Central Biotechnology*, Vol. 14, 2014, pp. 61.

[42]. E. Grosfeld, A. Stern, Observing Majorana bound states of Josephson vortices in topological superconductors, *PNAS*, Vol. 108, Issue 29, 2011, pp. 11810-11814.

[43]. R. Cosmic, H. Ikegami, A. Lin, K. Inomata, Circuit QED-based measurement of vortex lattice order in a Josephson junction array, *Physical Review B*, Vol 98, Issue 6, 2018, pp. 060501-060505.

[44]. J. Li, T. Neupert, B. Andrei Bernevig, A. Yazdani, Manipulating Majorana zero modes on atomic rings with an external magnetic field, *Nature Communication*, Vol. 7, 2016, 10395.

[45]. T. Watanabe-Nakayama, M. Itami, N. Kodera, *et al*., High-speed atomic force microscopy reveals strongly polarized movement of clostridial collagenase along collagen fibrils, *Scientific Reports*, Vol. 6, 2016.

[46]. M. F. Najafi, S. Zahri, F. Vahedi, *et al*., Which form of collagen is suitable for nerve cell culture? *Neural Regeneration Research*, Vol. 8, Issue 23, 2013, pp. 2165-2170.

[47]. W. Mckleroy, T-H Lee, K. Atahai, Always cleave up your mess: targeting collagen degradation to treat tissue fibrosis, *Am J Physiol Lung Cell Mol Physiol* Vol. 304, Issue 11, 2013, pp. L709-L721.

[48]. E. Takai, K. D. Costa, A. Shaheen, *et al*., Osteoblast elastic modulus measured by atomic force microscopy is substrate dependent, *Annals of Biomedical Engineering,* Vol. 33, Issue 7, 2005, pp. 963-971.

[49]. J. Clarke, A. I. Braginski, SQUID Handbook volume 1 and 2, *Wiley-VCH*, ISBN:3527-40229-2.

[50]. B. Back, W. H., Rippard, M. R. Pufall, *et. al*., Spin-transfer torque switch in nanopillar superconducting-magnetic hybrid Josephson Junction, *Physical Review Applied,* Vol. 3, 2015, 011001.

[51]. K. K. Likharev, Dynamics of Josephson junctions and circuits, *Gordon and Breach Science Publishers,* third printing, New Yonk, 1996.

[52]. M. Di Ventra, Y. V. Pershin, On the physical properties of memristive, memcapacitive and

meminductive systems, *Nanotechnology*, Vol. 24, Issue 25, 2013, 255201.

[53]. E. T. Chen, H. L. Pardue, Analytical Applications of Catalytic Properties of Modified-Cydodextrins, *Anal. Chem*, Vol. 65, Issue 19, 1993, pp. 2583-2587.
